ACS OMEGA

http://pubs.acs.org/journal/acsodf Article

Ultrasonic Clusterization Process to Prepare [$(NNCO)_6Co_4Cl_2$] as a Novel Double-Open-Co_4O_6 Cubane Cluster: SXRD Interactions, DFT, Physicochemical, Thermal Behaviors, and Biomimicking of Catecholase Activity

Abderrahim Titi,* Rachid Touzani, Anna Moliterni, Carlotta Giacobbe, Francesco Baldassarre, Mustapha Taleb, Nabil Al-Zaqri, Abdelkader Zarrouk, and Ismail Warad*

Cite This: *ACS Omega* 2022, 7, 32949−32958 Read Online

ACCESS | Metrics & More | Article Recommendations | Supporting Information

ABSTRACT: A novel double-open-cubane $(NNCO)_6Co_4Cl_2$ cluster with a Co_4O_6 core was made available under aqua-ultrasonic open atmosphere conditions for the first time. The ultrasonic clusterization of the (3,5-dimethyl-1*H*-pyrazol-1-yl)-methanol (NNCOH) ligand with $CoCl_2{\cdot}6H_2O$ salts in ethanol yielded a high-purity and high-yield cluster product. Energy-dispersive X-ray (EDX), Fourier transform infrared (FT-IR), and ultraviolet (UV)−visible techniques were used to elucidate the clusterization process. The double-open-Co_4O_6 cubane structure of the $(NNCO)_6Co_4Cl_2$ cluster was solved by synchrotron single-crystal X-ray diffraction (SXRD) and supported by density functional theory (DFT) optimization and thermogravimetric/differential TG (TG/DTG) measurements; moreover, the DFT structural parameters correlated with the ones determined by SXRD. Molecular electrostatic potential (MEP), Mulliken atomic charge/natural population analysis (MAC/NPA), highest occupied molecular orbital/lowest unoccupied molecular orbital (HOMO/LUMO), density of states (DOS), and GRD quantum analyses were computed at the DFT/B3LYP/6-311G(d,p) theory level. The thermal behavior of the cluster was characterized to support the formation of the Co_4O_6 core as a stable final product. The catalytic property of the $(NNCO)_6Co_4Cl_2$ cluster was predestined for the oxidation process of 3,5-DTBC diol (3,5-di-*tert*-butylbenzene-1,2-diol) to 3,5-DTBQ dione (3,5-di-*tert*-butylcyclohexa-3,5-diene-1,2-dione).

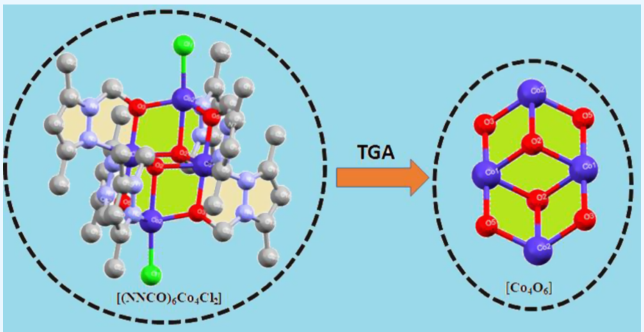

■ INTRODUCTION

Lately, exceptional care for the coordination chemistry domain has been focused on nitrogen heteroaromatic alcohol molecules like a family of commercially accessible compounds acquiring adaptability in complexation potentiality.[1−8] A large category of fascinating engineering of complexes is built from N,O^- donor alcohol building units.[9−14] Due to their optimal and fine characteristics, these molecules are extensively utilized like a crux for the construction of important materials based on polynuclear clusters.[15−18] The design and synthesis of polynuclear metal cluster-based coordination cages have attracted much interest, due to their esthetic structure and fascinating quantum mechanical properties, in applications including information storage, quantum computing, gas storage, drug delivery, conversion of CO_2, and crucial contribution in the catalysis of the splitting of water *via* enzymatic photosystem II {PS-II} of photosynthetic organisms.[19−21] This economic and ecofriendly model is the foundation for all envisioned solar fuel-based green energy strategies; accordingly, the biomodel is considered to be the efficient, simple, and clear starting phase for any bioinspired strategy.[22−25] As a result, the draft and assembly of the polynuclear metal cluster-based coordination cages are already charming and yet remain a synthetic challenge.[26−28] While most advances concerned the challenging preparation and characterization of the Mn-cluster oxygen evaluation conversion {OEC} mimic,[29−35] {Co_4O_6} cubane water oxidation catalysts {WOCs} appear to be preferred and ideal typical plan model systems for the essential oxidation reaction[36−40] and the creation of excellent photoanodes.[41−48]

In our recent work, we have synthesized several types of clusters based on cobalt, copper, and nickel ions with a general form {M_4O_6}, in addition to mixed samples with

Received: January 21, 2022
Accepted: June 14, 2022
Published: September 7, 2022

Scheme 1. Schematic Representation of the Synthesis of the $[(NNCO)_6Co_4Cl_2]$ Cluster

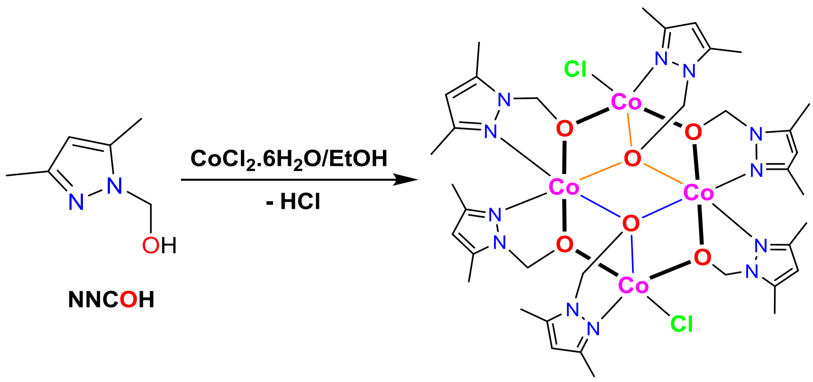

NNCOH

$(NNCO)_6Co_4Cl_2$

copper and cadmium like a bimetallic {Cd−O−Cu} double-open-cubane cluster using pyrazole alcohol compounds. The structures of most clusters were identified by single-crystal X-ray diffraction, and their oxidation properties were tested by conversion of catechol to *O*-quinone as an oxidation model.[49−55] In this context, the multifaceted double-open-cubane $[(NNCO)_6Co_4Cl_2]$ cluster was achieved by ultrasonic clusterization of the 1-hydroxymethyl-3,5-dimethylpyrazole (NNCOH) ligand with Co(II). The crystal structure of the desired $[(NNCO)_6Co_4Cl_2]$ cubane cluster was determined by synchrotron single-crystal X-ray diffraction (SXRD); moreover, several physicochemical and density functional theory (DFT) analyses in addition to the catalytic capacity of the cluster have been evaluated.

EXPERIMENTAL SECTION

Computational and SXRD. In the gaseous phase, all the DFT calculations were carried out *via* Gaussian09 software at the B3LYP/6-311G (d,p) level of theory.[56] Single-crystal X-ray diffraction experiments were performed at ID11, the Materials Science Beamline of the ESRF, Grenoble, France,[57] at room temperature, using a monochromatic beam with a wavelength (λ) of 29339 Å, (≈42.26 keV, relative bandwidth $\Delta\lambda/\lambda \sim 10^{-3}$) and a sample−detector distance of 118.81 mm. The beam was focused with a Si refractive compound lens system[58] to 500 nm. The detector beamline has been recently upgraded to a Dectris photon counting Eiger2 4M CdTe. The images were then converted into the "Esperanto" format using the script Eiger2esperanto, a portable image converter based on the FabIO library,[59] to export Eiger frames to a set of Esperanto frames, which can be imported into CrysalisPro software.[60] The converted detector images were successively indexed, and the intensities were estimated and corrected for Lorentz polarization effects using the CrysalisPro package. Scaling and correction for absorption were carried out by the semiempirical ABSPACK routine implemented in CrysalisPro. The crystal structure was solved by direct methods *via* the package SIR2019[61] and refined using full-matrix least-squares techniques using SHELXL2014/7.[62] All non-hydrogen atoms were refined anisotropically; the H atoms were placed at calculated positions, and their atomic coordinates were refined according to a riding model; the constraints on the isotropic U value of H atoms in the case of C−H and $C-H_2$ groups were $U_{iso}(H) = 1.2\ U_{eq}(C)$, and in the case of the methyl group, it was $U_{iso}(H) = 1.5\ U_{eq}(C)$. Additionally used computer programs were Mercury[63] for molecular graphics and WinGX[64] and publCIF[65] for preparing the published material.

Materials and Synthesis. Commercially available solvents and materials used in this study were purchased from Sigma-Aldrich.

Cluster synthesis: In ultrasonic medium, an ethanolic solution of $CoCl_2 \cdot 6H_2O$ (94.25 mg, 1.0 mmol in 20 mL) was mixed to a suspension solution of NNCOH (50 mg, 1.0 mmol in 12 mL). The change in the color of the mixture to dark brown by ∼2 h supported the possibility of ligand−metal clusterization; then, the reaction mixture was stirred for ∼5 min at RT before it was filtered. The filtrate was allowed to stand for 5 days, after the solvent was evaporated; suitable X-ray diffraction (XRD) crystals were collected with ∼81% yield.

RESULTS AND DISCUSSION

Synthesis, CHN-EA, and EDX of the Cluster. The multifaceted tetranuclear cubane $(NNCO)_6Co_4Cl_2$ cluster was synthesized by one to one equivalent amounts of $CoCl_2 \cdot 6H_2O$

Table 1. Cluster Refinement Data

chemical formula	$C_{36}H_{56}Cl_2C_{o4}N_{12}O_6$
M_r	1059.53
crystal system, space group	monoclinic, *P21/n*
temperature (K)	293
a, b, c (Å)	10.4826 (2), 18.5156 (2), 11.6440 (3)
β(°)	95.603 (2)
V(Å^3)	2249.20 (S)
Z	2
radiation type	synchrotron, λ = 0.29339 Å
μ (mm^{-1})	0.15
crystal size (mm)	0.09 × 0.06 × 0.02
absorption correction	empirical (using intensity measurements)
no. of measured, independent, and observed $[I > 2\sigma(I)]$ reflections	38068, 5410, 5008
R_{int}	0.059
$(\sin\theta/\lambda)_{max}$ (Å^{-1})	0.667
$R[F^2 > 2\sigma(F^2)]$, wR (F^2), S	0.051, 0.145, 1.14
no. of reflections	5410
no. of parameters	278
H-atom treatment	H-atom parameters constrained
$\Delta\rho_{max}$, $\Delta\rho_{min}$ (e Å^{-3})	1.01, −0.60
CCDC	2099518

https://doi.org/10.1021/acsomega.1c07032
ACS Omega 2022, 7, 32949−32958

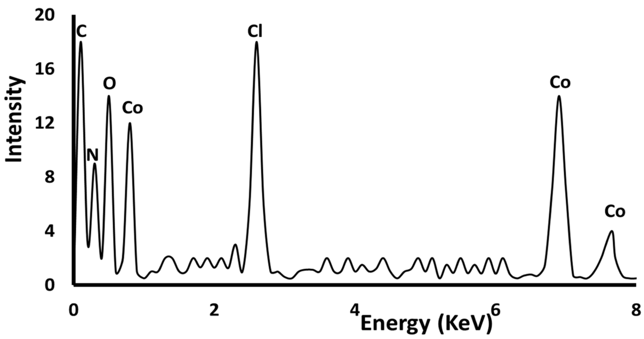

Figure 1. EDX of the $[(NNCO)_6Co_4Cl_2]$ cluster.

with 1-hydroxymethyl-3,5-dimethylpyrazole {NNCOH} under ambient conditions for 2 h (Scheme 1). The clusterization reaction to prepare the $[(NNCO)_6Co_4Cl_2]$ cluster was performed in ethanol and in free oxygen atmosphere, resulting in 80% yield with no side products. The clusterization reaction of NNCOH with $CoCl_2{\cdot}6H_2O$ was successfully monitored *via* FT-IR, UV−vis, and energy-dispersive X-ray (EDX) spectroscopy; the nonclassical double-open-Co_4O_6 cubane structure was confirmed by SXRD for the first time.

The atomic content of the $[(NNCO)_6Co_4Cl_2]$ cluster was verified by CHN-EA and EDX. The calculated CHN-EA data from $C_{36}H_{54}Cl_2Co_4N_{12}O_6$ molecular formula are C, 40.89; N, 15.89; and H, 5.15% and found to be C, 40.76; N, 15.69; and H, 5.24% (Table 1). EDX reflected only the signals of Co, C, O, N, and Cl that corresponded to the elemental composition of the $(NNCO)_6Co_4Cl_2$ desired cluster; moreover, a high degree of purity was achieved since no unknown signals were observed, as can be seen from Figure 1.

SXRD and DFT Optimization. The formation of the studied $[(NNCO)_6Co_4Cl_2]$ cluster was proved *via* SXRD and DFT optimization analysis (Figure 2); moreover, the comparison of the geometric parameters of the crystal

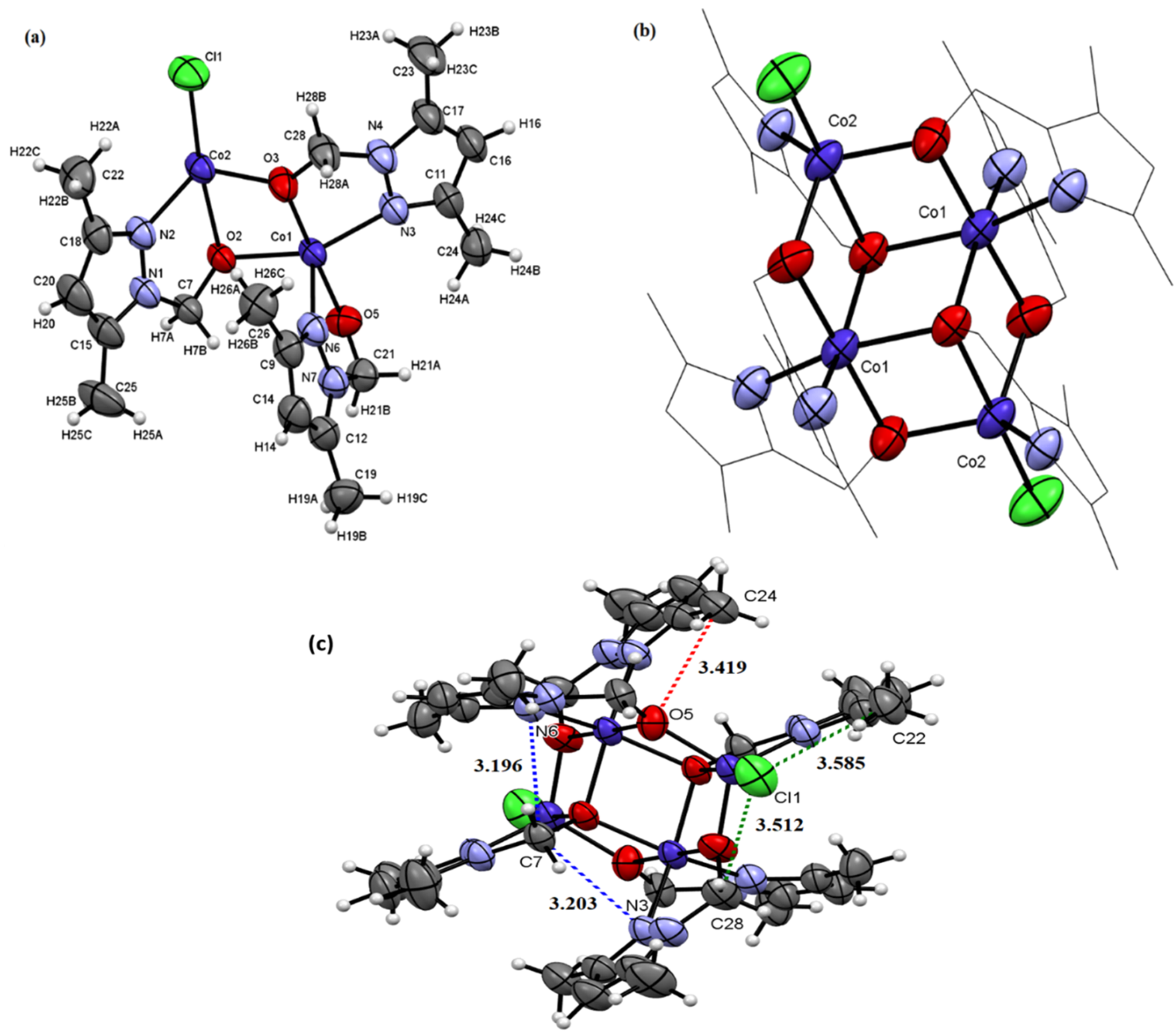

Figure 2. $[(NNCO)_6Co_4Cl_2]$ cluster: (a) View of the asymmetric unit with the atomic labeling scheme, (b) view of the local environment of the asymmetric unit showing the coordination of the Co(II) centers; and (c) ORTEP view showing all the H-bond types and lengths.

https://doi.org/10.1021/acsomega.1c07032
ACS Omega 2022, 7, 32949−32958

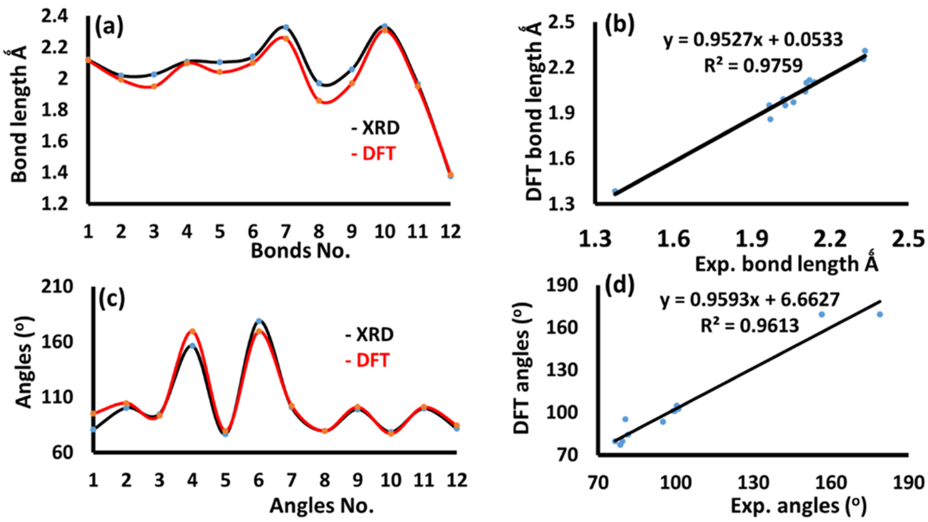

Figure 3. (a) Histogram of DFT/XRD bond distances and its (b) correlation coefficient and (c) histogram of angles and its (d) correlation coefficient.

Table 2. DFT/SXRD- Bonds Lengths (Å) and Angles (°)

no.	bond		XRD	DFT	no.	angles			XRD	DFT
1	Co1	O2	2.120(2)	2.1165	1	O2	Co1	O3	80.60(8)	95.12
2	Co1	O3	2.020(2)	1.8926	2	O2	Co1	O5	100.45(8)	104.66
3	Co1	O5	2.027(2)	1.9499	3	O2	Co1	N6	94.95(8)	93.54
4	Co1	O2	2.109(2)	1.9168	4	O2	Co1	N3	156.40(8)	169.42
5	Co1	N6	2.105(2)	2.0404	5	O2	Co1	O2	76.61(7)	79.61
6	Co1	N3	2.139(2)	1.919	6	O3	Co1	O5	178.90(8)	169.22
7	Co2	O2	2.326(2)	1.9165	7	O3	Co1	N6	100.99(9)	102.32
8	Co2	O3	1.970(2)	1.8592	8	O3	Co1	N3	79.35(9)	79.61
9	Co2	N2	2.059(2)	1.9191	9	O3	Co1	O2	99.04(8)	101.05
10	Co2	Cl1	2.333(1)	2.399	10	O5	Co1	N6	78.65(8)	77.24
11	Co2	O5	1.967(2)	1.9498	11	O5	Co1	N3	99.69(8)	101.05
12	O2	C7	1.376(3)	1.386	12	O5	Co1	O2	81.53(7)	84.35

Table 3. $[(NNCO)_6Co_4Cl_2]$ Cluster: H-Bond Interactions (Å, °)[a]

D—H···*A*	*D*—H	H···*A*	*D*···*A*	*D*—H···*A*
C7—H7*A*···N3	0.97	2.55	3.204 (4)	125
C7—H7*B*···N6[i]	0.97	2.53	3.196 (4)	126
C22—H22*A*···Cl1	0.96	2.66	3.585 (4)	163
C24—H24*A*···O5	0.96	2.64	3.419 (4)	139
C28—H28*B*···Cl1	0.97	2.91	3.512 (4)	121

[a]Symmetry code: (i) $-x + 2$, $-y$, $-60z + 2$.

structure determined by SXRD with those of the DFT-B3LYP/6-311G(d,p)-optimized structure is shown in Figures 3 and Tables 2 and 3. The tetranuclear Co(II) double-open-cubane $[(NNCO)_6Co_4Cl_2]$ cluster $C_{36}H_{56}Cl_2Co_4N_{12}O_6$ crystallizes as a dichloride neutral cluster, in the monoclinic crystal system, with the *P*21/*n* space group and unit cell parameters a = 10.4826 (2), b = 18.5156 (2), c = 11.6440 (3) Å, and β = 95.603 (2)°.

A view of the asymmetric unit (consisting of 2Co,1Cl, 3O, 6N, 18C, and 27H atoms) and its local environment showing the molecular structure of the $[(NNCO)_6Co_4Cl_2]$ cluster together with the double-open-cubane $[Co_4O_6]$ core is given in Figure 2a,b, respectively.

The asymmetric unit included two crystallographically independent cobalt(II) cations and three $NNCO^-$ anion ligands. One of these two Co(II) centers (i.e., Co1) was octahedrally coordinated (five of the six atoms at the vertices of the Co1-centered octahedron were symmetry-independent and the sixth one was symmetry-dependent), and the second Co(II) center had a trigonal bipyramid coordination. No Co—Co direct bonds were detected; four oxide atoms acted as trigonal bridges and two acted as tetrahedral bridges to connect Co(II) centers in the double-open-cubane core. The bond lengths concerning the Co1 atom belonged to the range 2.020(2)−2.139(2) Å, and the octahedron centered at Co1 was distorted, with two bond angles involving opposite vertices, N6—Co1—O2 and O2^i—Co1—N3, equal to 156.67 (8) and 156.41 (9), respectively, and far from the ideal value of 180° (*i.e.*, the typical value of undistorted octahedra). The presence of some H-bond interactions such as H...O, H...N, and H...Cl stabilizing the crystal packing was detected (see Table 3 and Figure 2c).

To study the compatibility of the crystal structural parameter data with their DFT- computational counterparts, a group of the selected bonds and angles (Table 2) was compared, and the results are illustrated in Figure 3. The XRD-structural parameters are in high agreement with the DFT-results, as can be deduced from Figure 3. The XRD and DFT bond distances were very similar, showing a linear relation with very good agreement (Figure 3a), characterized by a correlation coefficient of 0.976 (Figure 3b). Moreover,

https://doi.org/10.1021/acsomega.1c07032
ACS Omega 2022, 7, 32949−32958

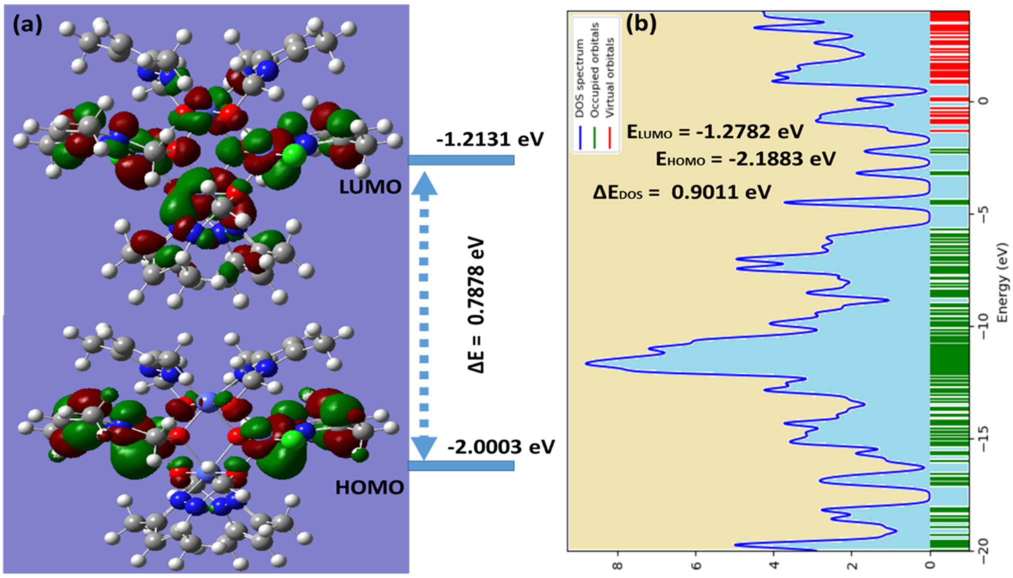

Figure 4. (a) Highest occupied molecular orbital/lowest unoccupied molecular orbital (HOMO/LUMO) and (b) DOS of the desired cluster.

XRD and DFT angles well agreed as shown in Figure 3c, with 0.961 correlation coefficient (Figure 3d).

FT-IR. The synthesis of the double-open-cubane $[(NNCO)_6Co_4Cl_2]$ cluster was tracked *via* FT-IR as seen in Figure 4. The IR spectra of the (NNCOH) free ligand before and after coordinating to the $CoCl_2{\cdot}6H_2O$ center to prepare the $[(NNCO)_6Co_4Cl_2]$ cluster have been recorded as seen in Figure S2 (see the Supporting Information). The biggest change that supported the clusterization interaction is the disappearance of the O−H band of the NNOH free ligand at 3161 cm^{-1} due to ionic bonding with the Co(II) center, resulting in a new Co−O band at 880 cm^{-1} in addition to the Co−N peak at 480 cm^{-1}. Moreover, taking into account the slight difference in the chemical shifts due to the bonding, various elongate frequency vibrations were apparent in the free ligand and the $[(NNCO)_6Co_4Cl_2]$ cluster, for example, C−H aliphatic and aromatic, C═C, N═N, C═C, C−O, Co−O, Co-N, and Co−Cl

UV−visible Behavior. To get more information about the absorbance behavior of the cluster, UV−vis of both the free ligand and the cluster was measured at 200−800 nm using methanol as a solvent. The free ligand in methanol reflected a π-to-π electron transfer at 280 nm; this peak is present also in the cluster at the same wavelength (Figure S3). Two new signs in the 600−750 nm range appeared when the free ligand clustered the $CoCl_2{\cdot}6H_2O$ to form the desired double-open-cubane $(NNCO)_6Co_4Cl_2$ cluster. The new two visible bands at 625 and 730 nm of the cluster can be attributed to metal d-to-d transitions as seen in Figure S3 (see the Supporting Information).

MEP and MAC/NPA Charges. The B3LYP/6311G(d,P) MEP map, natural population analysis (NPA), and Mulliken atomic charge (MAC) calculations of each atom in the $(NNCO)_6Co_4Cl_2$ cluster are illustrated in Figure S4 (see the Supporting Information) and Table 4. The result of MEP showed the presence of several positions that were characterized by the presence of electronic abundance nucleophiles (in red color) and the lack of electronic electrophiles (in blue color), but most of the functional groups were neutral green in color as shown in Figure S4a. The chlorine, oxygen, and nitrogen atoms have high nucleophilic properties; meanwhile, the cobalt and many hydrogen atoms have high electrophilic properties, as seen in Figure S4b. The MAC and NPA charges of each atom showed N, O, Cl, and some C atoms with negative charge also (Figure S4c and Table 4). Moreover, the Co and all H and most of the C atoms have positive charge. Moreover, a linear relation between MAC and NPA charges with a very good correlation coefficient (0.937) has been recorded, as shown in Figure S4d. The NPA/MAC charge MPE map results show strong correlation with the XRD interaction results.

HOMO → LUMO, DOS, and GRD. The highest occupied molecular orbital(HOMO), lowest unoccupied molecular orbital (LUMO), and frontier molecular orbitals played a considerable role in the evaluation of the optical and chemical relativities of the prepared molecules.[51−55] The $\Delta E_{HOMO/LUMO}$ energy bandgap is a helpful parameter for determining activity and stability molecular properties.[56] HOMO/LUMO shapes and energies have been characterized and then compared to DOS values; the elaborated HOMO and LUMO energy levels were found to be −2.0003 and −1.2131 eV, respectively. The calculations reflected a little amount of energy needed for the electron to be transferred from the HOMO to the LUMO with $\Delta E_{HOMO/LUMO}$ = 0.7878 eV (Figure 4a) that is consistent with a recently similar reported system.[53] Moreover, the energy gap was supported also *via* DOS calculation; the ΔE_{DOS} was 0.9011 eV that is very close to the $\Delta E_{HOMO/LUMO}$ result as represented in Figure 4b.

The main GRD parameters such as the electrophilicity (ω), softness (σ), chemical potential (μ), hardness (η), and electronegativity (χ) of the desired cluster were calculated *via*eqs 1−8 listed below, and the results are summarized in Table 5.

$$A\text{: electron affinity} = -E_{LUMO} \quad (1)$$

$$I\text{: ionization potential} = -E_{HOMO} \quad (2)$$

$$\chi\text{: absolute electronegativity} = (I + A)/2 \quad (3)$$

$$\Delta E_{gap}\text{: } \textit{energy gap} = E_{HOMO} - E_{LUMO} \quad (4)$$

$$\eta\text{: global hardness} = (I - A)/2 \quad (5)$$

https://doi.org/10.1021/acsomega.1c07032
ACS Omega 2022, 7, 32949−32958

Table 4. NPA and MAC Charge Population

no.	atom	MAC	NPA	no.	atom	MAC	NPA
1	O	−0.61192	−0.71664	58	N	−0.41002	−0.23065
2	O	−0.74039	−0.73435	59	C	−0.63462	−0.72028
3	O	−0.59988	−0.74906	60	C	−0.69888	−0.70459
4	Co	0.749812	0.90812	61	H	0.171175	0.2415
5	Co	1.313264	1.16056	62	H	0.15928	0.2415
6	Co	0.69633	0.9081	63	H	0.296498	0.25902
7	Co	1.198007	1.1355	64	H	0.191114	0.22977
8	O	−0.63176	−0.71662	65	H	0.210016	0.25055
9	O	−0.62157	−0.7491	66	H	0.277143	0.23287
10	O	−0.72395	−0.73435	67	H	0.206697	0.25355
11	N	−0.4359	−0.27402	68	H	0.201031	0.23852
12	N	−0.3588	−0.27405	69	H	0.191371	0.22977
13	C	0.228433	0.13631	70	H	0.303718	0.25054
14	C	−0.30213	−0.31998	71	H	0.223622	0.25904
15	C	0.347492	0.12595	72	H	0.217928	0.25356
16	N	−0.58023	−0.44436	73	H	0.219633	0.23853
17	C	0.212681	0.13629	74	H	0.212682	0.23287
18	C	−0.28762	−0.31998	75	H	0.323296	0.22879
19	C	0.348974	0.12592	76	H	0.264224	0.23983
20	N	−0.57808	−0.44439	77	H	0.234604	0.23982
21	C	−0.64475	−0.69986	78	H	0.321058	0.22878
22	C	−0.64813	−0.70736	79	H	0.19268	0.25315
23	C	−0.65064	−0.69987	80	H	0.371661	0.25979
24	C	−0.63962	−0.70736	81	H	0.22736	0.25138
25	Cl	−0.48207	−0.65481	82	H	0.20611	0.24657
26	C	−0.07934	0.06848	83	H	0.226174	0.2585
27	Cl	−0.48869	−0.65482	84	H	0.233265	0.25236
28	C	−0.08533	0.06846	85	H	0.249471	0.27029
29	N	−0.39312	−0.21297	86	H	0.192307	0.25315
30	C	0.268381	0.21808	87	H	0.225657	0.2585
31	C	−0.28125	−0.32847	88	H	0.227319	0.25236
32	C	0.359936	0.19949	89	H	0.238174	0.2703
33	N	−0.5649	−0.36161	90	H	0.202812	0.24658
34	C	−0.74427	−0.71543	91	H	0.314703	0.25978
35	C	−0.63493	−0.71983	92	H	0.261264	0.25137
36	N	−0.57786	−0.36164	93	H	0.361865	0.2573
37	C	0.283897	0.1995	94	H	0.252158	0.20743
38	C	−0.29263	−0.32846	95	H	0.235215	0.20743
39	C	0.275884	0.21812	96	H	0.26782	0.2573
40	N	−0.38704	−0.21297	97	H	0.278851	0.24014
41	C	−0.64342	−0.71983	98	H	0.259978	0.21831
42	C	−0.66239	−0.71542	99	H	0.187784	0.25352
43	C	−0.05727	0.04911	100	H	0.244682	0.24706
44	C	−0.02998	0.04909	101	H	0.220848	0.24252
45	C	0.025032	0.08098	102	H	0.327339	0.27302
46	N	−0.40379	−0.23065	103	H	0.234011	0.25553
47	C	0.237129	0.19036	104	H	0.225788	0.25943
48	C	−0.27384	−0.33345	105	H	0.231886	0.25634
49	C	0.295062	0.19908	106	H	0.255377	0.21832
50	N	−0.57309	−0.37329	107	H	0.278613	0.24015
51	C	−0.69018	−0.70457	108	H	0.185523	0.25352
52	C	−0.63256	−0.72028	109	H	0.246257	0.25634
53	C	−0.00798	0.08096	110	H	0.224411	0.25553
54	N	−0.56859	−0.37326	111	H	0.222022	0.25944
55	C	0.406898	0.19911	112	H	0.203215	0.24253
56	C	−0.29802	−0.33345	113	H	0.314655	0.27304
57	C	0.277697	0.19037	114	H	0.27	0.24705

$$\omega\text{: electrophilicity} = \mu^2/2\eta \quad (6)$$

$$\sigma\text{: global softness} = 1/\eta \quad (7)$$

https://doi.org/10.1021/acsomega.1c07032
ACS Omega 2022, 7, 32949−32958

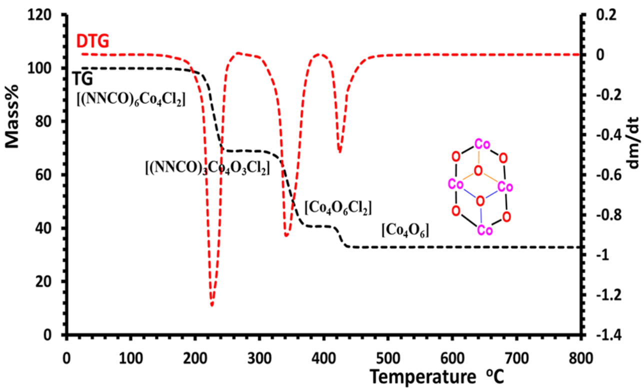

Figure 5. TG/DTG of the $(NNCO)_6Co_4Cl_2$ cluster with heating for 5 min.

$$\mu\text{: chemical potential} = -\chi \tag{8}$$

Thermal Behavior. The TG and DTG signals belonging to the $[(NNCO)_6Co_4Cl_2]$ cluster are illustrated in Figure 5. The cluster was decomposed via three steps; no small groups like methyl that decomposed early before 180 °C have been recorded. The first thermal decay of the cluster was recorded above 180–250 °C with T_{DTG} = 230 °C and 31% mass lost (theoretical 30.8%). Depending on the lost mass calculation, such a step can be attributed to 3NNC fragmented from the NNCO ligand resulting in the $[(NNCO)_6Co_4Cl_2] \rightarrow [(NNCO)_3Co_4O_3Cl_2]$ decomposition step. The second step was also due to the next 3NNC fragmented from the NNCO ligand resulting in $[(NNCO)_3Co_4O_3Cl_2] \rightarrow [Co_4O_6Cl_2]$

Table 5. GRD Quantum Parameters

GRD		value
global total energy	E_T	−8919.9848 a.u.
low unoccupied molecular orbital	LUMO	−0.0446 a.u.
high occupied molecular orbital	HOMO	−0.0735 a.u.
energy gap	ΔE_{gap}	0.0289 a.u.(0.7873 eV)
electron affinity	A	1.2131 eV
ionization potential	I	2.0003 eV
global hardness	η	0.3936 eV
global softness	σ	2.5406 eV
chemical potential	μ	−1.6123 eV
absolute electronegativity	Χ	1.6123 eV
electrophilicity	ω	3.2895 eV
dipole moment	u	1.4242 D

Scheme 2. Aerobic Oxidation of 3,5-DTBC to 3,5-BTBQ Catalyzed by the $(NNCO)_6Co_4Cl_2$ Cluster

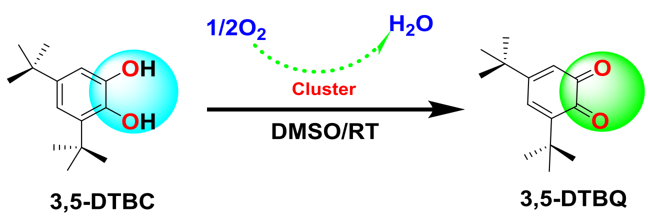

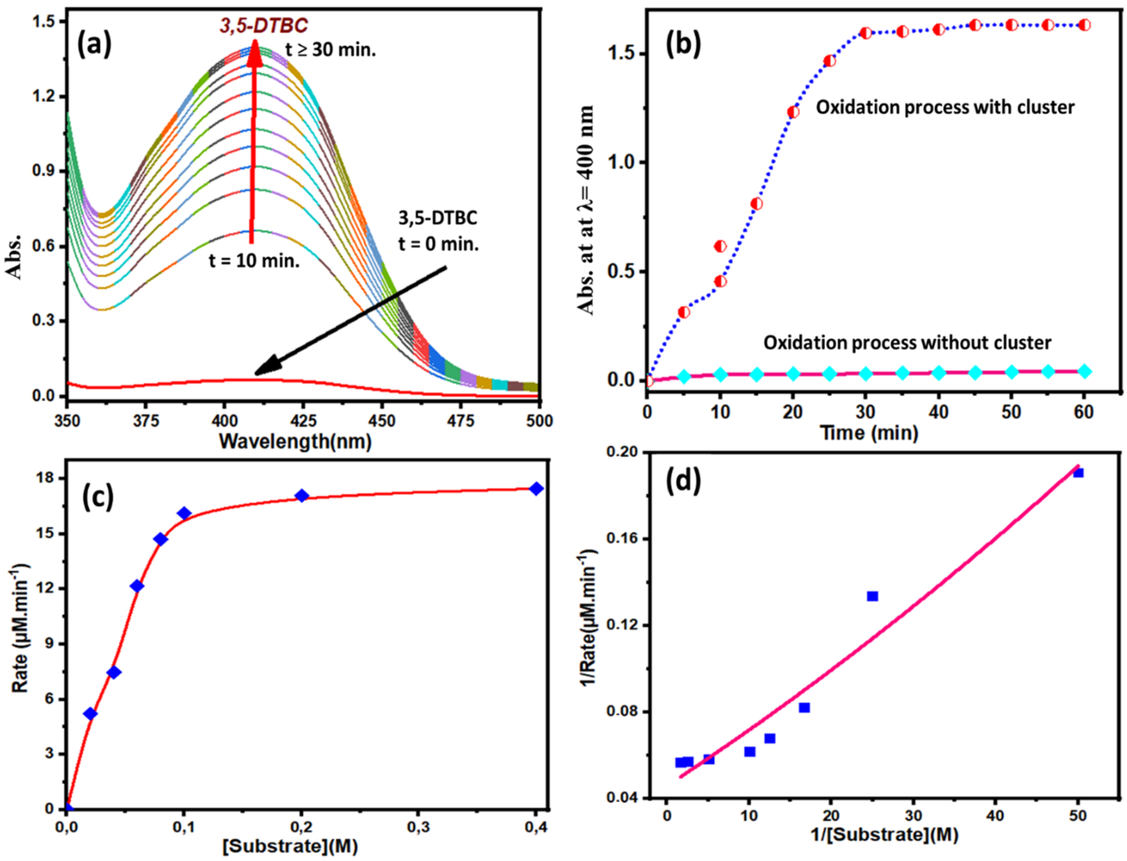

Figure 6. Aerobic oxidation of 0.1 M 3,5-DTBC using 1×10^{-5} M cluster as a catalyst in DMSO at RT, (a) Abs. vs wavelength (nm), the spectra were noted in the 5 min range, (b) Abs. (at λ = 400 nm) vs time for oxidation processes with and without the cluster, and (c) Michaelis–Menten rate vs [Sub.] and (d)1/rate vs 1/[Sub].

https://doi.org/10.1021/acsomega.1c07032
ACS Omega 2022, 7, 32949−32958

decomposed at 300−380 °C with T_{DTG} = 348 °C and 31% mass lost (theoretical 30.8%). The third step was attributed to loss of 2Cl resulting in the $[Co_4O_6Cl_2]$ → $[Co_4O_6]$ decomposition step from 420 to 460 °C with T_{DTG} = 424 °C and 7.1% mass lost (theoretical 6.8%). The stability (460−800 °C) and the quantity of the final mass residue (32.8%) greatly supported the possibility of cobalt oxide Co_4O_6 matrix formation (Figure 5).

Catalytic Activity of 3,5-DTB to 3,5-DTB Using the $(NNCO)_6Co_4Cl_2$ Cluster. One of the main objectives of this work is to test the ambient aerobic oxidation catalytic properties of 1,2-diol to 1,2-dione using the $(NNCO)_6Co_4Cl_2$ cluster, as seen in Scheme 2.

To achieve our objective, we mixed 0.1 M 3,5-di-*tert*-butylbenzene-1,2-diol (3,5-DTBC) with 1 × 10^{-5} M prepared cluster in the DMSO solvent under aerobic conditions for about 1h (Scheme 2). The production of the 3,5-di-tert-butylcyclohexa-3,5-diene-1,2-dione (3,5-DTBQ) product was tracked via UV−visible analysis at 400 nm in 350−500 nm (Abs. vs λ), as seen in Figure 6a. The catalytic capacity toward the oxidation of 3,5-DTBC was compared to a reference matrix with no cluster, as observed in Figure 6b. The sample containing the catalyst showed a very high activity; completeness was achieved within half an hour (Figure 6b), and meanwhile, no oxidation process was recorded under the same reaction conditions in the absence of the cluster.[48−53,66−68]

An important aspect of obtaining the catalyst kinetic data is the elucidation of pertinent kinetic parameters, K_m and V_{max}, across the aerobic oxidation process via Michaelis−Menten graphs, as seen in Figure 6c,d. In DMSO, promising V_{max} = 17.53 μmol L^{-1} min^{-1} and K_m = 0.04 mol L^{-1} values have been calculated for the aerobic RT oxidation of 0.1 M 3,5-DTBC using 1 × 10^{-5}M cluster concentration as a catalyst.

■ CONCLUSIONS

For the first time, a novel double-open-cubane $(NNCO)_6Co_4Cl_2$ cluster has been made available under ultrasonic media. The double-open Co_4O_6 cubane core in the $(NNCO)_6Co_4Cl_2$ cluster was clearly confirmed by SXRD and thermally proved by TG/DTG. The clusterization process of NNCOH with $CoCl_2$ salts was monitored by EDX, FT-IR, and UV−visible methods. In the crystal structure, the double-open-cubane cluster, both octahedral and trigonal bipyramids around the Co(II) center geometries, has been observed; moreover, the oxygen atoms acted as trigonal and tetrahedral bridges to connect the Co(II) centers. The SXRD characterization showed the presence of polar H...O, H...N, and H...Cl interactions that stabilized the Co_4O_6 core cluster lattice. The DFT optimization structural parameters match very well the corresponding SXRD-refined parameters; MAC/NPA and MEP electrostatics computations agree with the outcomes of the SXRD study, concerning the charge of each atom and their binding ability with their surroundings. GRD, HOMO/LUMO, and DOS quantum analyses confirmed the stability of the cluster and proved the convergence of the energy gap. The double-open-cubane $(NNCO)_6Co_4Cl_2$ cluster reflected a high thermal stability; three-step thermal decomposition was needed to reach the Co_4O_6 final stable core. The cluster showed a very high ability to oxidize 1,2-diol to 1,2-dione with a high TOF.

■ ASSOCIATED CONTENT

Supporting Information

The Supporting Information is available free of charge at https://pubs.acs.org/doi/10.1021/acsomega.1c07032.

IR analysis; UV−visible analysis; B3LYP/6311G (d,P) solid-MEP; and MEP, NPA/MAC charges, and MAC vs correlation (PDF)

■ AUTHOR INFORMATION

Corresponding Authors

Abderrahim Titi − *Laboratory of Applied and Environmental Chemistry, Mohammed First University, Oujda 60000, Morocco*; Email: titi_abderrahim1718@upm.ac.ma

Ismail Warad − *Department of Chemistry, AN-Najah National University, Nablus P400, Palestine*; orcid.org/0000-0001-8853-8961; Email: warad@najah.edu

Authors

Rachid Touzani − *Laboratory of Applied and Environmental Chemistry, Mohammed First University, Oujda 60000, Morocco*; orcid.org/0000-0001-7333-697X

Anna Moliterni − *Institute of Crystallography, CNR, Bari 70126, Italy*

Carlotta Giacobbe − *European Synchrotron Radiation Facility, Grenoble 38040, France*

Francesco Baldassarre − *Institute of Crystallography, CNR, Bari 70126, Italy*; orcid.org/0000-0001-9045-3764

Mustapha Taleb − *Laboratory of Engineering, Organometallic, Molecular and Environment (LIMOME), Faculty of Science, Université Sidi Mohamed Ben Abdellah, Fez 30000, Morocco*

Nabil Al-Zaqri − *Department of Chemistry, College of Science, King Saud University, Riyadh 11451, Saudi Arabia*

Abdelkader Zarrouk − *Laboratory of Materials, Nanotechnology, and Environment, Faculty of Sciences, Mohammed V University in Rabat, Agdal-Rabat 11000, Morocco*; orcid.org/0000-0002-5495-2125

Complete contact information is available at: https://pubs.acs.org/10.1021/acsomega.1c07032

Notes

The authors declare no competing financial interest.

■ ACKNOWLEDGMENTS

This work is a bilateral project between the CNR, Italy, and the CNRST, Morocco, (project 2020/2021, CUP B54I20000340001, IC-CNR Bari, Italy, A.M., and UMP Oujda, Morocco, R.T.). A.M. and F.B. are grateful to R Lassandro for his technical assistance and to Dr. Caterina Chiarella for her contribution in the bilateral project administration. The authors would like to thank Dr. Jonathan Wright for the provision of in-house time at ID11. The authors extend their appreciation to the Researchers Supporting Project number (RSP-2021/396), King Saud University, Riyadh, Saudi Arabia.

■ REFERENCES

(1) Dvořáčková, O.; Zdeněk, C. Tuning the Reactivity and Bonding Properties of Metal Square-Planar Complexes by the Substitution(s) on the Trans-Coordinated Pyridine Ring. *ACS Omega* **2020**, *5*, 11768−11783.

(2) Segľa, P.; Kuchtanin, V.; Tatarko, M.; Švorec, J.; Moncol, J.; Valko, M. Structural study and magnetic properties of copper (II) thiophene-2-carboxylate with 4-pyridinemethanol and isonicotinamide. *Chem. Pap.* **2018**, *72*, 863−876.
(3) Qin, L.; Zhang, H. L.; Zhai, Y. Q.; Nojiri, H.; Schröder, C.; Zheng, Y. Z. A giant spin molecule with ninety-six parallel-unpaired electrons. *iScience* **2021**, *24*, No. 102350.
(4) Masternak, J.; Zienkiewicz-Machnik, M.; Kowalik, M.; Jabłońska-Wawrzycka, A.; Rogala, P.; Adach, A.; Barszcz, B. Recent advances in coordination chemistry of metal complexes based on nitrogen heteroaromatic alcohols. Synthesis, structures and potential applications. *Coord. Chem. Rev.* **2016**, *327*−*328*, 242−270.
(5) Masternak, J.; Zienkiewicz-Machnik, M.; Łakomska, I.; Hodorowicz, M.; Kazimierczuk, K.; Nosek, M.; Barszcz, B.; et al. Synthesis and Structure of Novel Copper (II) Complexes with N, O- or N, N-Donors as Radical Scavengers and a Functional Model of the Active Sites in Metalloenzymes. *Int. J. Mol. Sci.* **2021**, *22*, No. 7286.
(6) Amani, V.; Sharafie, D.; Hamedani, N. F.; Naseh, M. Zinc (II) and mercury (II) iodide complexes containing 2-pyridinealdoxime compound: Synthesis, characterization, crystal structure determination and DFT study. *J. Iran. Chem. Soc.* **2020**, *17*, 441−451.
(7) Icsel, C.; Yilmaz, V. T.; Ari, F.; Ulukaya, E.; Harrison, W. T. trans-Dichloridopalladium (II) and platinum (II) complexes with 2-(hydroxymethyl) pyridine and 2-(2-hydroxyethyl) pyridine: synthesis, structural characterization, DNA binding and in vitro cytotoxicity studies. *Eur. J. Med. Chem.* **2013**, *60*, 386−394.
(8) Jabłońska-Wawrzycka, A.; Barszcz, B.; Zienkiewicz, M.; Hodorowicz, M.; Jezierska, J.; Stadnicka, K.; Lechowicz, Ł.; Kaca, W. Eight-and six-coordinated Mn(II) complexes of heteroaromatic alcohol and aldehyde: Crystal structure, spectral, magnetic, thermal and antibacterial activity studies. *Spectrochim. Acta, Part A* **2014**, *129*, 632−642.
(9) Zienkiewicz, M.; Jabłońska-Wawrzycka, A.; Szlachetko, J.; Kayser, Y.; Stadnicka, K.; Sawka-Dobrowolska, W.; Sá, J.; et al. Effective catalytic disproportionation of aqueous H_2O_2 with di-and mono-nuclear manganese(II) complexes containing pyridine alcohol ligands. *Dalton Trans.* **2014**, *43*, 8599−8608.
(10) Zienkiewicz, M.; Szlachetko, J.; Lothschütz, C.; Hodorowicz, M.; Jabłońska-Wawrzycka, A.; Sá, J.; Barszcz, B. A novel single-site manganese(II) complex of a pyridine derivative as a catalase mimetic for disproportionation of H_2O_2 in water. *Dalton Trans.* **2013**, *42*, 7761−7767.
(11) Zhu, W.; Yang, Z.; Yasin, A.; Liu, Y.; Zhang, L. Preparation of Poly (acrylic acid-acrylamide/starch) Composite and Its Adsorption Properties for Mercury (II). *Materials* **2021**, *14*, No. 3277.
(12) Kim, E.; Woo, H. Y.; Kim, S.; Lee, H.; Kim, D.; Lee, H. Synthesis and X-ray crystal structure of derivatives from the N, N-bis (1H-pyrazolyl-1-methyl) aniline (dichloro) Zn (II) complex: Substituent effects on the phenyl ring versus the pyrazole ring. *Polyhedron* **2012**, *42*, 135−141.
(13) Otero, A.; Fernández-Baeza, J.; Lara-Sánchez, A.; Sánchez-Barba, L. F. Metal complexes with heteroscorpionate ligands based on the bis (pyrazol-1-yl) methane moiety: Catalytic chemistry. *Coord. Chem. Rev.* **2013**, *257*, 1806−1868.
(14) Xue, F.; Zhao, J.; Hor, T. A. Cross-coupling of alkyl halides with aryl or alkyl Grignards catalyzed by dinuclear Ni(II) complexes containing functionalized tripodal amine-pyrazolyl ligands. *Dalton Trans.* **2013**, *42*, 5150−5158.
(15) Yang, M.; Park, W. J.; Yoon, K. B.; Jeong, J. H.; Lee, H. Synthesis, characterization, and MMA polymerization activity of tetrahedral Co(II) complex bearing N, N-bis (1-pyrazolyl) methyl ligand based on aniline moiety. *Inorg. Chem. Commun.* **2011**, *14*, 189−193.
(16) Boussalah, N.; Touzani, R.; Bouabdallah, I.; El Kadiri, S.; Ghalem, S. Synthesis, structure and catalytic properties of tripodal amino-acid derivatized pyrazole-based ligands. *J. Mol. Catal. A: Chem.* **2009**, *306*, 113−117.
(17) Scarpellini, M.; Gätjens, J.; Martin, O. J.; Kampf, J. W.; Sherman, S. E.; Pecoraro, V. L. Modeling the resting state of oxalate oxidase and oxalate decarboxylase enzymes. *Inorg. Chem.* **2008**, *47*, 3584−3593.
(18) Scarpellini, M.; Wu, A. J.; Kampf, J. W.; Pecoraro, V. L. Corroborative models of the cobalt (II) inhibited Fe/Mn superoxide dismutase. *Inorg. Chem.* **2005**, *44*, 5001−5010.
(19) McEvoy, J. P.; Brudvig, G. W. Water-splitting chemistry of photosystem II. *Chem. Rev.* **2006**, *106*, 4455−4483.
(20) Najafpour, M. M.; Madadkhani, S.; Akbarian, S.; Hołyńska, M.; Kompany-Zareh, M.; Tomo, T.; Allakhverdiev, S. I.; et al. A new strategy to make an artificial enzyme: photosystem II around nanosized manganese oxide. *Catal. Sci. Technol.* **2017**, *7*, 4451−4461.
(21) Cox, N.; Pantazis, D. A.; Neese, F.; Lubitz, W. Biological water oxidation. *Acc. Chem. Res.* **2013**, *46*, 1588−1596.
(22) Schwiedrzik, L.; Brieskorn, V.; González, L. Flexibility Enhances Reactivity: Redox Isomerism and Jahn−Teller Effects in a Bioinspired Mn4O4 Cubane Water Oxidation Catalyst. *ACS Catal.* **2021**, *11*, 13320−13329.
(23) Dau, H.; Limberg, C.; Reier, T.; Risch, M.; Roggan, S.; Strasser, P. The mechanism of water oxidation: from electrolysis via homogeneous to biological catalysis. *ChemCatChem* **2010**, *2*, 724−761.
(24) Najafpour, M. M.; Govindjee. Oxygen evolving complex in Photosystem II: Better than excellent. *Dalton Trans.* **2011**, *40*, 9076−9084.
(25) Najafpour, M. M.; Moghaddam, A. N.; Allakhverdiev, S. I.; Govindjee. Biological water oxidation: lessons from nature. *Biochim. Biophys. Acta, Bioenerg.* **2012**, *1817*, 1110−1121.
(26) Zhang, C.; Chen, C.; Dong, H.; Shen, J. R.; Dau, H.; Zhao, J. A synthetic Mn4Ca-cluster mimicking the oxygen-evolving center of photosynthesis. *Science* **2015**, *348*, 690−693.
(27) Gerey, B.; Gouré, E.; Fortage, J.; Pécaut, J.; Collomb, M. N. Manganese-calcium/strontium heterometallic compounds and their relevance for the oxygen-evolving center of photosystem II. *Coord. Chem. Rev.* **2016**, *319*, 1−24.
(28) Lin, P. H.; Takase, M. K.; Agapie, T. Investigations of the effect of the non-manganese metal in heterometallic-oxido cluster models of the oxygen evolving complex of photosystem II: lanthanides as substitutes for calcium. *Inorg. Chem.* **2015**, *54*, 59−64.
(29) Scheurer, A.; Korzekwa, J.; Nakajima, T.; Hampel, F.; Buling, A.; Derks, C.; Meyer, K.; et al. Synthesis, Magnetic Properties, and X-ray Spectroscopy of Divalent Cobalt (II) and Nickel (II) Cubanes $[MII_4(HL_2)_4(OAc)_4]$. *Eur. J. Inorg. Chem.* **2015**, *2015*, 1872−1901.
(30) Davis, K. M.; Palenik, M. C.; Yan, L.; Smith, P. F.; Seidler, G. T.; Dismukes, G. C.; Pushkar, Y. N. X-ray emission spectroscopy of Mn coordination complexes toward interpreting the electronic structure of the oxygen-evolving complex of photosystem II. *J. Phys. Chem. C.* **2016**, *120*, 3326−3333.
(31) Liao, R. Z.; Siegbahn, P. E. Mechanism for OO bond formation in a biomimetic tetranuclear manganese cluster−A density functional theory study. *J. Photochem. Photobiol., B* **2015**, *152*, 162−172.
(32) Lin, P. H.; Tsui, E. Y.; Habib, F.; Murugesu, M.; Agapie, T. Effect of the Mn Oxidation State on Single-Molecule-Magnet Properties: MnIII vs MnIV in Biologically Inspired DyMn3O4 Cubanes. *Inorg. Chem.* **2016**, *55*, 6095−6099.
(33) Berardi, S.; La Ganga, G.; Natali, M.; Bazzan, I.; Puntoriero, F.; Sartorel, A.; Bonchio, M.; et al. Photocatalytic water oxidation: tuning light-induced electron transfer by molecular Co_4O_4 cores. *J. Am. Chem. Soc.* **2012**, *134*, 11104−11107.
(34) McCool, N. S.; Robinson, D. M.; Sheats, J. E.; Dismukes, G. C. A Co_4O_4 "cubane" water oxidation catalyst inspired by photosynthesis. *J. Am. Chem. Soc.* **2011**, *133*, 11446−11449.
(35) La Ganga, G.; Nardo, V. M.; Cordaro, M.; Natali, M.; Vitale, S.; Licciardello, A.; Nastasi, F.; Campagna, S. A functionalized, ethynyl-decorated, tetracobalt(III) cubane molecular catalyst for photoinduced water oxidation. *Dalton Trans.* **2014**, *43*, 14926−14930.
(36) Ullman, A. M.; Liu, Y.; Huynh, M.; Bediako, D. K.; Wang, H.; Anderson, B. L.; Nocera, D. G.; et al. Water oxidation catalysis by Co

(II) impurities in $Co(III)_4O_4$ cubanes. *J. Am. Chem. Soc.* **2014**, *136*, 17681−17688.
(37) Zhou, X.; Li, F.; Li, H.; Zhang, B.; Yu, F.; Sun, L. Photocatalytic water oxidation by molecular assemblies based on cobalt catalysts. *ChemSusChem* **2014**, *7*, 2453−2456.
(38) La Ganga, G.; Puntoriero, F.; Campagna, S.; Bazzan, I.; Berardi, S.; Bonchio, M.; Scandola, F.; et al. Light-driven water oxidation with a molecular tetra-cobalt(III) cubane cluster. *Faraday Discuss.* **2012**, *155*, 177−190.
(39) Genoni, A.; La Ganga, G.; Volpe, A.; Puntoriero, F.; Di Valentin, M.; Bonchio, M.; Natali, M.; Sartorel, A. Water oxidation catalysis upon evolution of molecular Co(III) cubanes in aqueous media. *Faraday Discuss.* **2015**, *185*, 121−141.
(40) Chen, H. C.; Reek, J. N.; Williams, R. M.; Brouwer, A. M. Halogenated earth abundant metalloporphyrins as photostable sensitizers for visible-light-driven water oxidation in a neutral phosphate buffer solution. *Phys. Chem. Chem. Phys.* **2016**, *18*, 15191−15198.
(41) Smith, P. F.; Hunt, L.; Laursen, A. B.; Sagar, V.; Kaushik, S.; Calvinho, K. U.; Dismukes, G. C.; et al. Water oxidation by the $[Co_4O_4(OAc)_4(py)_4]^+$ cubium is initiated by OH−addition. *J. Am. Chem. Soc.* **2015**, *137*, 15460−15468.
(42) Nguyen, A. I.; Ziegler, M. S.; Oña-Burgos, P.; Sturzbecher-Hohne, M.; Kim, W.; Bellone, D. E.; Tilley, T. D. Mechanistic investigations of water oxidation by a molecular cobalt oxide analogue: Evidence for a highly oxidized intermediate and exclusive terminal oxo participation. *J. Am. Chem. Soc.* **2015**, *137*, 12865−12872.
(43) Wang, Y.; Li, F.; Zhou, X.; Yu, F.; Du, J.; Bai, L.; Sun, L. Highly efficient photoelectrochemical water splitting with an immobilized molecular Co_4O_4 cubane catalyst. *Angew. Chem.* **2017**, *129*, 7015−7019.
(44) Swierk, J. R.; Mallouk, T. E. Design and development of photoanodes for water-splitting dye-sensitized photoelectrochemical cells. *Chem. Soc. Rev.* **2013**, *42*, 2357−2387.
(45) Yuan, H.; De'Andra, L. N.; Seymour, L. A.; Metz, A.; Cropek, D.; Holder, A. A.; Ofoli, R. Y. Characterization and functional assessment of a cobalt(III)-oxo cubane cluster water oxidation catalyst immobilized on ITO. *Catal. Commun.* **2014**, *56*, 76−80.
(46) Li, X.; Clatworthy, E. B.; Masters, A. F.; Maschmeyer, T. Molecular cobalt clusters as precursors of distinct active species in electrochemical, photochemical, and photoelectrochemical water oxidation reactions in phosphate electrolytes. *Chem. - Eur. J.* **2015**, *21*, 16578−16584.
(47) Wang, Y.; Li, F.; Li, H.; Bai, L.; Sun, L. Photocatalytic water oxidation via combination of BiVO 4−RGO and molecular cobalt catalysts. *Chem. Commun.* **2016**, *52*, 3050−3053.
(48) Titi, A.; Shiga, T.; Oshio, H.; Touzani, R.; Hammouti, B.; Mouslim, M.; Warad, I. Synthesis of novel Cl2Co4L6 clusterusing 1-hydroxymethyl-3, 5-dimethylpyrazole (LH) ligand: Crystal structure, spectral, thermal, Hirschfeld surface analysis and catalytic oxidation evaluation. *J. Mol. Struct.* **2020**, *1199*, No. 126995.
(49) Titi, A.; Oshio, H.; Touzani, R.; Mouslim, M.; Zarrouk, A.; Hammouti, B.; Warad, I.; et al. Synthesis and XRD of Novel Ni 4 (μ 3-O) 4 Twist Cubane Cluster Using Three NNO Mixed Ligands: Hirshfeld, Spectral, Thermal and Oxidation Properties. *J. Cluster Sci.* **2020**, *32*, 227−234.
(50) Titi, A.; Messali, M.; Touzani, R.; Fettouhi, M.; Zarrouk, A.; Al-Zaqri, N.; Warad, I.; et al. Synthesis of Novel Tetra (μ3-Methoxo) Bridged with [Cu (II)-O-Cd (II)] Double-Open-Cubane Cluster: XRD/HSA-Interactions, Spectral and Oxidizing Properties. *Int. J. Mol. Sci.* **2020**, *21*, No. 8787.
(51) Titi, A.; Almutairi, S. M.; Alrefaei, A. F.; Manoharadas, S.; Alqurashy, B. A.; Sahu, P. K.; Ali, I.; et al. Novel phenethylimidazolium based ionic liquids: Design, microwave synthesis, in-silico, modeling and biological evaluation studies. *J. Mol. Liq.* **2020**, *315*, No. 113778.
(52) Titi, A.; Messali, M.; Alqurashy, B. A.; Touzani, R.; Shiga, T.; Oshio, H.; Hadda, T. B.; et al. Synthesis, characterization, X-Ray crystal study and bioctivities of pyrazole derivatives: Identification of antitumor, antifungal and antibacterial pharmacophore sites. *J. Mol. Struct.* **2020**, *1205*, No. 127625.
(53) Titi, A.; Warad, I.; Almutairi, S. M.; Fettouhi, M.; Messali, M.; Aljuhani, A.; Touzani, R.; Zarrouk, A. One-pot liquid microwave-assisted green synthesis of neutral trans-Cl2Cu(NNOH)2: XRD/HSA-interactions, antifungal and antibacterial evaluations. *Inorg. Chem. Commun.* **2020**, *122*, No. 108292.
(54) Saleem, F. A.; Musameh, S.; Sawafta, A.; Brandao, P.; Tavares, C. J.; Ferdov, S.; Barakat, A.; Ali, A.; Al-Noaimi, M.; Warad, I. Diethylenetriamine/diamines/copper (II) complexes [Cu(dien)-(NN)]Br2: Synthesis, solvatochromism, thermal, electrochemistry, single crystal, Hirshfeld surface analysis and antibacterial. *Arabian J. Chem.* **2017**, *10*, 845−854.
(55) Rbaa, M.; Ouakki, M.; Galai, M.; Berisha, A.; Lakhrissi, B.; Jama, C.; Warad, I.; Zarrouk, A. Simple preparation and characterization of novel 8-Hydroxyquinoline derivatives as effective acid corrosion inhibitor for mild steel: Experimental and theoretical studies. *Colloids Surf., A* **2020**, *602*, No. 125094.
(56) Zandi, H.; Harismah, K. Density functional theory analyses of non-covalent complex formation of 6-thioguanine and coronene. *Lab-in-Silico* **2021**, *2*, 57−62.
(57) Wright, J.; Giacobbe, C.; Majkut, M. New opportunities at the Materials Science Beamline at ESRF to exploit high energy nano-focus X-ray beams. *Curr. Opin. Solid State Mater. Sci.* **2020**, *24*, No. 100818.
(58) Snigirev, A.; Kohn, V.; Snigireva, I.; Lengeler, B. A compound refractive lens for focusing high-energy X-rays. *Nature* **1996**, *384*, 49−51.
(59) Knudsen, E. B.; Sørensen, H. O.; Wright, J. P.; Goret, G.; Kieffer, J. FabIO: easy access to two-dimensional X-ray detector images in Python. *J. Appl. Crystallogr.* **2013**, *46*, 537−539.
(60) CrysAlis, P. R. O.*Rigaku Oxford Diffraction*; Yarnton, Oxfordshire: England, 2015.
(61) Burla, M. C.; Caliandro, R.; Carrozzini, B.; Cascarano, G. L.; Cuocci, C.; Giacovazzo, C.; Mallamo, M.; Mazzone, A.; Polidori, G. Crystal structure determination and refinement via SIR2014. *J. Appl. Crystallogr.* **2015**, *48*, 306−309.
(62) Sheldrick, G. M. Crystal structure refinement with SHELXL. *Acta Crystallogr., Sect. C: Struct. Chem.* **2015**, *71*, 3−8.
(63) Macrae, C. F.; Sovago, I.; Cottrell, S. J.; Galek, P. T. A.; McCabe, P.; Pidcock, E.; Platings, M.; Shields, G. P.; Stevens, J. S.; Towler, M.; Wood, P. A. Mercury 4.0: From visualization to analysis, design and prediction. *J. Appl. Crystallogr.* **2020**, *53*, 226−235.
(64) Farrugia, L. J. WinGX and ORTEP for Windows: an update. *J. Appl. Crystallogr.* **2012**, *45*, 849−854.
(65) Westrip, S. P. publCIF: software for editing, validating and formatting crystallographic information files. *J. Appl. Crystallogr.* **2010**, *43*, 920−925.
(66) Shit, M.; Maity, S.; Bera, S.; Mudi, P. K.; Biswas, B.; Weyhermüller, T.; Ghosh, P. Nickel(II) di-aqua complex containing a water cluster: synthesis, X-ray structure and catecholase activity. *New J. Chem.* **2021**, *45*, 2221−2227.
(67) Pal, C. P.; Mahato, S.; Yadav, H. R.; Shit, M.; Choudhury, A. R.; Biswas, B. Bio-mimetic of catecholase and phosphatase activity by a tetra-iron (III) cluster. *Polyhedron* **2019**, *174*, No. 114156.
(68) De, A.; Dey, D.; Yadav, H.; Maji, M.; Rane, V.; Kadam, R. M.; Choudhury, A. R.; Biswas, B. Unprecedented hetero-geometric discrete copper (II) complexes: Crystal structure and bio-mimicking of Catecholase activity. *J. Chem. Sci.* **2016**, *128*, 1775−1782.

https://doi.org/10.1021/acsomega.1c07032
ACS Omega 2022, 7, 32949−32958